RSC Advances

ROYAL SOCIETY OF CHEMISTRY

PAPER

View Article Online
View Journal | View Issue

Cite this: *RSC Adv.*, 2026, **16**, 18709

DNA/BSA binding, antidiabetic and antioxidant studies of copper(II) complexes derived from *ONO*-tridentate Schiff bases and diimines as auxiliary ligands

Segun D. Oladipo,*[a] Adesola A. Adeleke,[b] Kolawole A. Olofisan,[c] Bernard Omondi[b] and Robert C. Luckay *[a]

Six new copper(II) complexes with general molecular formula [Cu**L1**(Phen)] (**1**), [Cu**L2**(Phen)] (**2**), [Cu**L3**(Phen)] (**3**), [Cu**L1**(DM-Phen)] (**4**), [Cu**L2**(DM-Phen)] (**5**) and [Cu**L3**(DM-Phen)] (**6**) (**L** = (*E*)-1-(((4-chloro-2-hydroxyphenyl)imino)methyl)naphthalen-2-ol (**L1**), (*E*)-1-(((2-hydroxy-5-methylphenyl)imino)methyl)naphthalen-2-ol (**L2**), (*E*)-1-(((2-hydroxy-4-nitrophenyl)imino)methyl)naphthalen-2-ol (**L3**), Phen = 1,10-phenanthroline and DM-Phen = 2,9-dimethyl-1,10-phenanthroline) have been synthesized and characterized by spectroscopic as well as crystallographic techniques. Molecular structures of **2**, **4**, **5** and **6** revealed that they are mononuclear species where the copper(II) center is five-coordinated to a pair of oxygen atoms as well as one nitrogen atom from the ligands (**L1–L3**) and to a pair of nitrogen atoms from the auxiliary ligand (Phen or DM-Phen) conforming to a distorted square pyramid. The binding affinities of ligands **L1–L3** and copper(II) complexes **1–6** with calf thymus DNA (ctDNA) and bovine serum albumin (BSA) were evaluated using UV-visible absorption spectroscopy. For ctDNA, all compounds showed hypochromism and bathochromic shifts suggesting intercalative binding, with K_b values ranging from 1.49×10^4 to 2.74×10^5 M^{-1}. The complexes exhibited 3–18-fold higher affinity than ligands, especially those with 2,9-dimethyl-1,10-phenanthroline coligands. BSA titrations of complexes **1–6** revealed hyperchromic shifts at ~280 nm, with K_b values of 9.59×10^4 to 2.41×10^5 M^{-1}. These moderate-to-strong bindings were enhanced by lipophilic substituents that promote hydrophobic and π-stacking interactions in protein pockets. All of the compounds inhibit α-amylase better than acarbose with complex **5** (IC_{50} = 0.274 mM) showing the highest activity. For the α-glucosidase assay, only complexes **2** (IC_{50} = 0.055 mM) and **4** (IC_{50} = 0.054 mM) outshined acarbose (IC_{50} = 0.059 mM) while other compounds showed moderate to good α-glucosidase inhibition activity. Antioxidant activities of the free ligands showed better activity than that of the metal complexes with none of the compounds performing better than quercetin in all of the assays explored for this study.

Received 25th February 2026
Accepted 1st April 2026

DOI: 10.1039/d6ra01650b

rsc.li/rsc-advances

1 Introduction

The research on the design and development of metallodrugs with multifunctional therapeutic activities continues to gain significant interest in the field of bioinorganic and medicinal chemistry.[1,2] Among metal ions explored in metal-based drugs, copper has been unique due to its important role in biological systems. Copper exists in crucial enzymes (*i.e.*, ceruloplasmin, laccase, superoxide dismutase, ascorbate oxidase, among others).[3,4] These enzymes are essential in energy metabolism and nervous system development.[5] It is found in humans either as Cu^{2+} (oxidized form) or Cu^{+} (reduced form). While high doses of copper are toxic, copper(II) ions are less toxic than copper(I) ions at appropriate concentrations. This is because, in aqueous solutions, copper(II) is the most stable oxidation state, while copper(I) is highly prone to oxidation (less stable) and not easy to develop into reliable oral medication. In pharmaceuticals, copper-based drugs or supplements are mainly copper(II) salts or complexes, *i.e.*, copper(II) glycinate and copper(II) citrate, both common in supplements.[6,7] Copper(II) participates in diverse physiological processes, including enzymatic catalysis, electron transfer, and oxidative stress regulation, making copper-based complexes potential candidates for therapeutic application.[8]

Schiff base ligands have been widely explored as chelate ligands in coordination chemistry.[9,10] They are well known for

[a]*Department of Chemistry and Polymer Science, Stellenbosch University, Private Bag X1, Matieland 7602, South Africa. E-mail: segun.oladipo@oouagoiwoye.edu.ng; rcluckay@sun.ac.za*

[b]*School of Agriculture and Science, Discipline of Chemistry, University of Kwazulu-Natal, Private Bag X54001, Durban, South Africa*

[c]*Department of Pharmacology, University of Free State, Bloemfontein 9300, South Africa*

their structural versatility, robust metal-binding ability, and tunable electronic properties. The bio-active azomethine functional group, which allows nucleophilic and electrophilic reactions at the electron-rich nitrogen and electron-deficient carbon atoms, respectively, has been linked to the inherent therapeutic qualities of Schiff bases.[11,12] Copper(II) complexes derived from Schiff bases have been reported to display a myriad of medicinal properties, which include anticancer, antioxidant, antimicrobial, and antifungal with enhanced medicinal activity compared to the free ligands.[13,14] However, the incorporation of planar nitrogen heterocyclic (N-heterocyclic) *i.e.*, 2,2-bipyridine, 1,10-phenanthroline, and 2,9-dimethyl-1,10-phenanthroline, is known to further enhance the biological activities of copper(II) complexes. These N-heterocyclic ligands are well known for their strong π–π stacking interaction with nucleic acid–base pairs of DNA, hence facilitating DNA intercalation.[15]

DNA binding studies play an important role in developing DNA molecule probes and chemotherapeutics.[16,17] It also helps in understanding the mechanisms of action of metal-based drugs, as interaction with DNA can influence replication and transcription processes.[18] Strong binding affinities for DNA *via* intercalative, groove-binding, or electrostatic modes have been shown by copper(II) complexes, especially those with Schiff bases and N-heterocyclic ligands and these affinities do corroborate with biological activities.[19–23] Hence, the need to evaluate the DNA binding potential of newly synthesized compounds is crucial to elucidate possible mechanisms of biological activity. Similarly, BSA binding studies are equally vital, as bovine serum albumin (BSA), a model plasma protein, transports metal complexes in blood, influencing their bioavailability, distribution, and toxicity. Copper(II) Schiff base complexes often exhibit strong BSA affinity through hydrophobic interactions or hydrogen bonding with its Sudlow sites, which correlates with enhanced therapeutic efficacy.[24] These studies provide insights into drug–protein interactions, complementing DNA binding data for multifunctional agents.

In addition to the DNA and BSA binding potential of copper(II) complexes, they have also attracted interest as antidiabetic agents, through the inhibition of carbohydrate-hydrolyzing enzymes such as α-glucosidase and α-amylase enzymes.[25–27] Inhibiting these enzymes can reduce postprandial hyperglycemia by retarding the rate at which dietary starch breaks down to glucose in the body and this has been validated as an effective strategy to manage diabetes.[28] It is important to note that, drugs like acarbose and miglitol have been successfully used to treat diabetes by acting as α-glucosidase and α-amylase inhibitors. However, adverse effects associated with their usage *i.e.*, stomach discomfort, meteorism, and diarrhea due to undigested carbohydrate fermenting in the bowel, have significantly decreased their use as antidiabetic medication.[29,30] Hence, the need for new α-glucosidase and α-amylase inhibitors with little or no side effects.

Interestingly, oxidative stress has been associated with the progression and complications of diabetes, highlighting the relevance of antioxidant activity in potential antidiabetic drugs.[31–33] Aside from that free radicals are closely linked to the cause of diabetes, they are also associated to deadly diseases such as liver cirrhosis, cancer, atherosclerosis among others.[34] Hence, an antioxidant drug could play a crucial chemoprotective role in the treatment of diabetes and other diseases. Copper(II) complexes do display radical scavenging activity due to facile redox cyclic between Cu(II) and Cu(I) states, contributing to their therapeutic relevance.[14] Copper(II) complexes derived from Schiff bases have demonstrated significant antioxidant activities in multiple radical scavenging assays.[9,14,35]

In this study, the ligand design was based on introducing controlled variations in electronic, steric and physicochemical properties. Chloro and nitro substituents were selected as electron-withdrawing groups, while the methyl group was included as an electron-donating substituent to facilitate comparison of electronic effects on the resulting copper(II) complexes. Furthermore, 1,10-phenanthroline and 2,9-dimethyl-1,10-phenanthroline were used as co-ligands to probe steric and lipophilic influences, as methyl substitution at the 2 and 9 positions may increase steric hindrances and hydrophobicity. These variations were considered in relation to their potential impact on biological interactions, including DNA binding affinity and inhibitory activity against α-amylase and α-glucosidase enzymes. Herein, we report the synthesis and characterization of copper(II) complexes derived from *ONO*-donor Schiff base ligands and N-heterocyclic (1,10-phenanthroline or 2,9-dimethyl-1,10-phenanthroline) as coligands. Their DNA/BSA binding, antidiabetic, and antioxidant potential are investigated to evaluate their suitability as multifunctional bioactive agents.

2 Experimental

2.1 Reagents

The reagents used for the preparation of the metal complexes are 1,10-phenanthroline (≥99%), 2,9-dimethyl-1,10-phenanthroline (≥98%), 2-hydroxy-4-nitroaniline (98%), 2-amino-5-chlorophenol (97%), 2-hydroxy-5-methylaniline (97%), acetic acid, and copper(II) acetate monohydrate (≥98%). Solvents such as dimethyl sulfoxide (DMSO), methanol and diethyl ether are A.C.S. grade and used as obtained. All reagents are purchased from Merck.

2.2 Instrumentation

The FT-IR spectra for complexes **1–6** were obtained using a PerkinElmer Universal A.T.R. spectrum 100 FT-IR spectrometer, and the elemental/combustion analysis for the complexes was carried out using a Vario elemental E.L. cube CHNS analyser. Shimadzu UV-Vis-NIR spectrophotometer was used to obtain the UV-Visible spectra of all the complexes and Waters Synapt G2 coupled to a Waters UPLC., ESI probe, ESI Positive, Cone Voltage 15 V was used to analyze the mass spectra for the complexes. The JEOL FA200 spectrometer was used to record the electron paramagnetic resonance (EPR) spectra for compounds **1–6**.

2.3 Preparation of complexes 1–6

We have previously reported the synthetic procedures as well as fully characterized the Schiff base ligands **L1–L3** used in the

preparation of complexes **1–6**.[36] For the preparation of complexes **1–6**, we followed the procedure reported by Kiran *et al.*[37] with slight modification. 0.751 mmol (0.150 g) of copper(II) acetate monohydrate was dissolved in 20 mL of methanol in 100 mL round bottom flask and stirred until complete dissolution. Thereafter, 0.751 mmol of methanolic solution of 1,10-phenanthroline or 2,9-dimethyl-1,10-phenanthroline was added to the copper(II) salt solution and heated to around 40–50 °C while stirring vigorously for 1 h. For the 1,10-phenanthroline, the solution turned deep blue, while the one for 2,9-dimethyl-1,10-phenanthroline, it turned light green. 0.751 mmol of **L1–L3** dissolved in 20 mL of dimethyl sulfoxide is added to the reaction mixture in a round bottom flask and further stirred for another 1 h. After 10 min of stirring, a reddish-brown precipitate crashed out of the reaction mixture, which was later washed with methanol and rinsed four times with diethyl ether. The obtained products were dried in an oven at 60–70 °C.

2.3.1 Synthesis of Cu(L1)(Phen) (1). FT-IR ν (cm^{-1}): (νC–H = 3054), (νC=N = 1600), (νC=C = 1576), (νC–N = 1395), (νC–O = 1291), and (νCu–N = 557). ES-TOF MS: m/z(%): $[M + H]^+$, 539.0454, $[M + Na\text{-naph}]^+$, 436.9912 MS calc. analysis: 538.04 (100.0%), 540.04 (44.6%). Anal. calc. for $C_{29}H_{18}ClCuN_3O_2$0.5-C_2H_6OS: C, 62.28, H, 3.66, N, 7.26. Found: C, 62.30, H, 3.89, N, 7.46.

2.3.2 Synthesis of Cu(L2)(Phen) (2). FT-IR ν (cm^{-1}): (νC–H = 3051), (νC=*N* = 1600), (νC=C = 1583), (νC–N = 1388), (νC–O = 1299), and (νCu–N = 557). ES-TOF MS: m/z(%): $[M + H]^+$, 519.100, $[M + Na\text{-naph}]^+$, 417.0460 MS calc. analysis: 518.09 (100.0%), 520.09 (44.6%), 519.10 (32.4%). Anal. calc. for $C_{30}H_{21}CuN_3O_2$: C, 69.42, H, 4.08, N, 8.10. Found: C, 69.30, H, 3.42, N, 8.04.

2.3.3 Synthesis of Cu(L3)(Phen) (3). FT-IR ν (cm^{-1}): (νC–H = 3054), (νC=N = 1598), (νC=C = 1584), (νC–N = 1365), (νC–O = 1284), and (νCu–N = 572). ES-TOF MS: m/z(%): $[M + H]^+$, 550.0701, $[M + Na\text{-naph}]^+$, 448.0151 MS calc. analysis: 549.06 (100.0%), 551.06 (44.6%), 550.07 (31.4%). Anal. calc. for C_{29}-$H_{18}CuN_4O_4$0.5C_2H_6OS: C, 61.17, H, 3.59, N, 9.51. Found: C, 61.29, H, 3.87, N, 9.82.

2.3.4 Synthesis of Cu(L1)(DMPhen) (4). FT-IR ν (cm^{-1}): (νC–H = 3100–3000), (νC=N = 1601), (νC=C = 1587), (νC–N = 1394), (νC–O = 1290), and (νCu–N = 569). ES-TOF MS: m/z(%): $[M + H]^+$, 567.0773, $[M + Na\text{-ArCl}]^+$, 479.1292 MS calc. analysis: 566.07 (100.0%), 568.07 (44.6%), 567.07 (33.5%). Anal. calc. for $C_{29}H_{18}CuN_4O_4$0.5C_2H_6OS: C, 64.22, H, 4.06, N, 7.11. Found: C, 64.44, H, 4.26, N, 7.24.

2.3.5 Synthesis of Cu(L2)(DMPhen) (5). FT-IR ν (cm^{-1}): (νC–H = 3048), (νC=N = 1601), (νC=C = 1585), (νC–N = 1389), (νC–O = 1275), and (νCu–N = 555). ES-TOF MS: m/z(%): $[M + Na\text{-}ArCH_3]^+$, 479.1297 $[M + H]^+$, 547.12 MS calc. analysis: 546.1 (100.0%), 548.12 (44.6%), 547.13 (34.6%). Anal. calc. for C_{32}-$H_{25}CuN_3O_2$0.3C_2H_6OS: C, 68.63, H, 4.73, N, 7.38. Found: C, 68.30, H, 4.78, N, 7.24.

2.3.6 Synthesis of Cu(L3)(DMPhen) (6). FT-IR ν (cm^{-1}): (νC–H = 3054), (νC=N = 1600), (νC=C = 1587), (νC–N = 1367), (νC–O = 1277), and (νCu–N = 571). ES-TOF MS: m/z(%): $[M + Na\text{-}ArNO_2]^+$, 479.1288 MS calc. analysis: 577.09 (100.0%), 579.09 (44.6%), 578.10 (33.5%). Anal. calc. for $C_{31}H_{22}CuN_4O_4$0.5C_2H_6-OS: C, 62.88, H, 4.08, N, 9.08. Found: C, 62.74, H, 3.92, N, 9.21.

2.4 Single crystal X-ray crystallography

Crystals with dimensions of 0.258 × 0.075 × 0.032 mm^3 (for **2**), 0.231 × 0.117 × 0.107 mm^3 (for **4**), 0.483 × 0.221 × 0.074 mm^3 (for **5**), and 0.153 × 0.140 × 0.039 mm^3 (for **6**) were mounted on a Bruker DUO Apex II X-ray diffractometer equipped with an INCOATEC IμS HB microfocus tube (MoKα radiation λ = 0.71073 Å) fitted with a multilayer monochromator. Data were captured with a CCD (charge-coupled device) area detector. Data collection was carried out at 100 K using an Oxford Cryosystems cryostat (700 series Cryostream Plus) attached to the diffractometer. Data collection and reduction were carried out using the Bruker software package *APEX4*,[38] using standard procedures. All structures were solved and refined using *SHELX*-2016[39] employed within the *X-Seed*[40] environment. Hydrogen atoms were placed in calculated positions using riding models. Diagrams for the crystal structures were obtained by *Mercury* software.[41] Table 1 details the structural data together with the refinement parameters.

2.5 DNA binding study

The DNA binding study was done using modified literature procedures.[42,43] UV-visible absorption spectroscopy was employed to investigate the binding affinity of ligands **L1–L3** and complexes **1–6** with calf thymus DNA (ctDNA). The ctDNA stock solution was prepared by dissolving an appropriate amount in phosphate buffer saline (pH 7.2), with its concentration quantified spectrophotometrically using the molar absorptivity coefficient $\varepsilon_{260} = 6600\ M^{-1}\ cm^{-1}$. The purity of the ctDNA solution was confirmed by a UV absorbance ratio $A_{260}/A_{280} > 1.8$, verifying the absence of protein contamination. Binding interactions were evaluated by maintaining a fixed compound concentration of 40 μM while incrementally adding ctDNA (0–25 μM). The compound-DNA mixtures were incubated for 5 min at 25 °C prior to recording absorption spectra. Intrinsic binding constants K_b were determined by nonlinear fitting of the data to the Wolfe–Shimmer equation (eqn (1)). The experiments were performed in triplicate to confirm the precision and accuracy of the procedure and in all the experiments on the interaction of the compounds with ctDNA, the final concentration of DMSO in the incubation mixture was ~2% (v/v).

$$\frac{1}{(A - A_0)} = \frac{1}{(A_{max} - A_0)} + \frac{1}{K_b(A_{max} - A_0)[complex]_n} \quad (1)$$

where A is the absorbance recorded in the presence of an added guest, A_0 is the absorbance of the receptor in the absence of a guest, and A_{max} is the absorbance in the presence of added $[complex]_n$.

2.6 Protein binding studies

The interactions of complexes **1–6** were performed using the UV-vis absorption titration method.[44] BSA stock solutions were prepared by dissolving the protein in phosphate-buffered saline

Table 1 X-ray crystal structural data together with refinement parameters collections for complexes **2**, **4**, **5** and **6**

	2	**4**	**5**	**6**
Empirical formula	$C_{31}H_{23}Cl_2CuN_3O_2$	$C_{32}H_{23}Cl_4CuN_3O_2$	$C_{33}H_{29}CuN_3O_3$	$C_{32}H_{24}Cl_2CuN_4O_4$
Formula weight	603.96	686.87	579.13	662.99
Crystal system	Monoclinic	Monoclinic	Monoclinic	Triclinic
Space group	$P2_1/c$	$P2_1/c$	$P2_1/n$	$P\bar{1}$
a/Å	10.1131(6)	10.3155(3)	9.6459(6)	7.418(4)
b/Å	18.2779(10)	22.5459(6)	20.2675(13)	13.351(7)
c/Å	14.6964(8)	13.4635(4)	14.4479(9)	15.437(8)
α/°	90	90	90	93.220(16)
β/°	105.1330(10)	107.6710(10)	108.352(2)	103.676(15)
γ/°	90	90	90	103.705(16)
Volume/Å^3	2622.4(3)	2983.49(15)	2680.9(3)	1433.1(14)
Z	4	4	4	2
ρ_{calc}/g cm^{-3}	1.530	1.529	1.435	1.536
μ/mm^{-1}	1.072	1.126	0.856	0.995
F(000)	1236	1396	1204	678
Crystal size/mm^3	0.258 × 0.075 × 0.032	0.231 × 0.117 × 0.107	0.483 × 0.221 × 0.074	0.153 × 0.140 × 0.039
2Θ range for data collection/°	1.817 to 26.410	1.806 to 26.386	1.793 to 26.420	1.581 to 26.582
Index ranges	$-12 \le h \le 12$	$-12 \le h \le 12$	$-12 \le h \le 11$	$-9 \le h \le 9$
	$-22 \le k \le 22$	$-28 \le k \le 28$	$-25 \le k \le 25$	$-16 \le k \le 16$
	$-18 \le l \le 18$	$-16 \le l \le 16$	$-18 \le l \le 17$	$-19 \le l \le 19$
Reflections collected	53 446	67 118	64 228	29 441
Independent reflections	5383 [$R_{int} = 0.0653$]	6105 [$R_{int} = 0.0410$]	5477 [$R_{int} = 0.0477$]	5874 [$R_{int} = 0.0949$]
Data/restraints/parameters	5383/0/353	6105/0/381	5477/0/366	5874/718/418
Goodness-of-fit on F^2	1.056	1.031	1.040	0.992
Final R indexes [$I \ge 2\sigma(I)$]	$R_1 = 0.0391$, w$R_2 = 0.0910$	$R_1 = 0.0424$, w$R_2 = 0.1077$	$R_1 = 0.0479$, w$R_2 = 0.1139$	$R_1 = 0.0590$, w$R_2 = 0.1492$
Final R indexes [all data]	$R_1 = 0.0602$, w$R_2 = 0.1008$	$R_1 = 0.0610$, w$R_2 = 0.1216$	$R_1 = 0.0614$, w$R_2 = 0.1210$	$R_1 = 0.0951$, w$R_2 = 0.1714$
Largest diff. peak and hole (e Å^{-3})	0.453 and −0.399	0.516 and −0.370	1.063 and −0.442	0.399 and −0.949

(pH 7.2) at 25 °C under constant stirring, with concentrations determined spectrophotometrically using the molar absorptivity coefficient $\varepsilon_{280} = 44\,300$ M^{-1} cm^{-1}. The complexes' stock solutions (1×10^3 mM) were dissolved in DMSO. Titrations were done by adding varying complex concentrations (0–10 μM) to a fixed BSA concentration (6 μM), followed by 5 min incubation at 25 °C. The experiments were performed in triplicate to confirm the precision and accuracy of the procedure, and in all the experiments on the interaction of the compounds with ctDNA, the final concentration of DMSO in the incubation mixture was ∼1% (v/v). Absorption at $\lambda_{max} = 280$ nm was measured, and the binding constant K_b was calculated using the Benesi–Hildebrand equation (eqn (2)) from the intercept to the slope ratio of $1/[A - A_0]$ *vs.* 1/[complex].

$$\frac{1}{(A - A_0)} = \frac{1}{(A - A_0)} + \frac{1}{K_b(A - A_0)[\text{complex}]_n} \quad (2)$$

where A and A_0 represent the absorbance of BSA in the presence and absence of complex, respectively.

2.7 Antidiabetes studies

2.7.1 Inhibition of α-amylase activity. α-Amylase is a calcium metalloenzyme and a key digestive enzyme that breaks down carbohydrates into glucose causing postprandial blood sugar spikes in diabetes patients. Inhibiting this enzyme is a crucial therapeutic strategy for type 2 diabetes. The ability of acarbose and the compounds to inhibit the α-amylase was determined using the method according to Ibitoye *et al.*[45] with slight modification. 25 μL of varied concentrations of the compounds were added to 175 μL of distilled water in a test tube. After adding 200 μL of the 2.5 mg mL^{-1} pancreatic α-amylase solution in 0.1 M sodium phosphate buffer (pH 6.8), the resulting solution was incubated for 20 minutes at 37 °C. Then, 0.15 mL of a 1% starch solution was added to initiate the enzyme's catalytic activity. After allowing the reaction to proceed for 15 minutes under the same previous conditions, it was terminated by adding 0.4 mL of dinitrosalicylic acid reagent. The whole solution was boiled in a water bath for 10 minutes before 1 mL of distilled water was added. Finally, the absorbance of the coloured solution was read in a microplate reader at 540 nm against a blank solution lacking the test samples.

2.7.2 Inhibition of α-glucosidase activity. α-Glucosidase is an enzyme in the small intestine that breaks down complex carbohydrates into glucose, causing post-meal blood sugar spikes. This enzyme is responsible for the final step of carbohydrate digestion into glucose, allowing absorption into the bloodstream. Inhibiting α-glucosidase in the human body results in lower and slower rise in blood glucose level after meals.[30] The ability of acarbose and the compounds to inhibit α-glucosidase activity was determined using the protocol according to Olofinsan *et al.*[46] where *p*-nitrophenyl-α-D-glucopyranoside (pNPG) was employed as enzyme substrate. 25 μL of each compound or acarbose was diluted with 100 μL of distilled water in a 96-well plate. The solution was then incubated with the enzyme solution, which contained 0.1 M sodium phosphate buffer (pH 6.8) with yeast α-glucosidase (1.5 U mL^{-1}). The

mixture was incubated for 15 minutes at 37 °C. The enzyme reaction was initiated by adding pNPG (2 mg mL^{-1}), and the reaction was monitored for 1 minute. The optical density was then measured in a microplate reader at 405 nm.

2.8 Antioxidant studies

2.8.1 Nitric oxide production inhibitory capacity. While sodium nitroprusside (Na_2[Fe(CN)5NO]) at physiological pH releases nitric oxide, the ability of the compounds to inhibit this process was determined using the method described by Beseni *et al.*[47] with minor modifications. 100 μL of the compounds or quercetin solutions at 250–2000 μM were incubated with a Na_2[Fe(CN)5NO] solution (5 mM) in PBS for 1 hour and 30 minutes at 37 °C in Eppendorf tubes. 50 μL of each resulting solution was pipetted to the 96-well plate in triplicate before the addition of 50 μL of Griess reagent. The optical density of the pink chromogen developed after this step was measured in a microplate reader at 540 nm against a blank sample containing distilled water instead of the test samples.

2.8.2 Free radical neutralising ability. The interaction of the synthesized compound with 2,2-diphenyl-1-picrylhydrazyl (DPPH) was conducted according to the protocol of Changlian *et al.*[48] with little modification. DPPH powder was initially dissolved in methanol to achieve a final concentration of 0.3 mM in an amber bottle. Then, 100 μL of the compound's solution and the free radical solution were incubated in a 96-well plate in the dark for 20 minutes. The degree of bleaching of the initial colour of the DPPH solution was measured in microplate reader at 517 nm against a blank solution lacking the test compound or quercetin.

2.8.3 Ferric ion reductive capacity. The ability of the compounds to reduce ferric ion in comparison with quercetin at 250–2000 μM concentration was assessed using the Beseni *et al.*[47] method with slight modifications. 0.1 mL of each compound solution was added to an equal volume of potassium ferricyanide, followed by an hour of equilibration at 50 °C in an incubator. After adding 50 μL of distilled water and the same volume of 10% trichloroacetic acid, the mixture was subjected to centrifugation at 4000*g* for 15 minutes. Then, 150 μL of each sample was added to 50 μL of $FeCl_3$ (0.1%) in a 96-well plate. The absorbance of the resulting mixture was read at 700 nm in a microplate reader.

3 Results and discussion

3.1 Preparation of complexes 1–6

The free ligands **L1–L3** explored in synthesizing complexes **1–6** were prepared by the condensation reaction between 2-hydroxy-1-napthaldehyde and respective primary amines *viz*; 2-amino-5-chlorophenol (**L1**), 2-hydroxy-5-methylaniline (**L2**) and 2-hydroxy-4-nitroaniline (**L3**) in ratio 1 : 1 at room temperature. The reaction between ligand (**L1**/**L2**/**L3**), copper(II) salt ($Cu(CH_3COO)_2.H_2O$) and *N,N′*-adducts ligands (1,10-phenanthroline or 2,9-dimethyl-1,10-phenanthroline) at 40–50 °C in 1 : 1 : 1 respectively affords complexes **1–6** (Scheme 1) in good yield. The resulting copper(II) complexes are reddish brown in colour and very stable at room temperature. Generally, the complexes dissolve readily in DMSO, dichloromethane as well as chloromethane, while they do not dissolve readily in tetrahydrofuran and protic solvents *i.e.*, ethanol and methanol. They are completely insoluble in hexane.

3.2 Spectroscopic elucidation of complexes 1–6

3.2.1 FT-IR and UV-visible. FT-IR spectra for complexes **1–6** were obtained within the range of 4000–500 cm^{-1} in order to identify the core functional groups available in the compounds as well as compare them to the ones for the free ligands which have been previously reported. The azomethine stretching vibrational band ($\nu C{=}N)_{str}$ which is the diagnostic peak for Schiff base derivatives was observed around 1598–1601 cm^{-1} in **1–6** and when compared to the ones for the free ligands, **L1–L3** (1612–1616 cm^{-1}) previously reported, it appeared at a lower vibrational frequency, and this confirmed the involvement of the azomethine nitrogen atom (CH=**N**) in coordination to the copper(II) metal center. Furthermore, the absence of a pronounced vibrational broad band within the region of 3200–3500 cm^{-1} unravel the deprotonation of the hydroxyl group and coordination of the resulting phenolate as well as naphtholate oxygen to the copper(II) center. The vibrational bands which were observed around 500–650 cm^{-1} in the spectra of all the complexes might be due to the formation of Cu–O and Cu–N bonds.

The electronic absorption spectra of the compounds were recorded within the range of 200–800 nm using the dichloromethane solution of the respective compound (Fig. 1). In the ultraviolet region, one intense band as well as one weak shoulder band were observed around 265–270 nm and 360–365 nm and these bands can be attributed to $\pi \rightarrow \pi^*$ and $n \rightarrow \pi^*$, respectively due to the intra-ligand transition within the complexes. In the visible region, an intense band can also be observed around 400–600 nm in the spectra of complexes **1–6**, and this is due to metal-to-ligand charge transfer (LMCT). It could be observed that the absorption band for complexes **3** and **6** with nitro ($-NO_2$) moiety appeared at a longer wavelength. This is because the nitro group is a strong electron-withdrawing group which acts as a strong chromophore that elongates the absorption range into longer wavelengths by lowering the electronic energy gap. A very weak band due to d–d transitions were also observed around 600–650 nm in the electronic spectra of the complexes.

3.2.2 Electron spin resonance (ESR) spectroscopy. The paramagnetic nature of complexes **1–6** were confirmed by ESR techniques, which were carried out by recording the ESR spectra at X-band frequency for the complexes in their powder state and are shown in Fig. 2 and S8. It could be observed that all the spectra are of strong intensity, affirming the ESR sensitivity of copper(II) complexes, and they are also known to possess characteristic g-values. A *g*-factor of approximately 2.0 (1.9728 for **1**, 1.9817 for **2**, 1.9901 for **3**, 1.9788 for **4**, 1.9684 for **5** and 1.9844 for **6**) which is equivalent to that of a free electron ($g = 2.0023$). The absence of forbidden $\Delta M_s = \pm 2$ line (half field signal) in all the spectra rules out the possibility of a dimer resulting from a pronounced Cu···Cu interaction.[49,50]

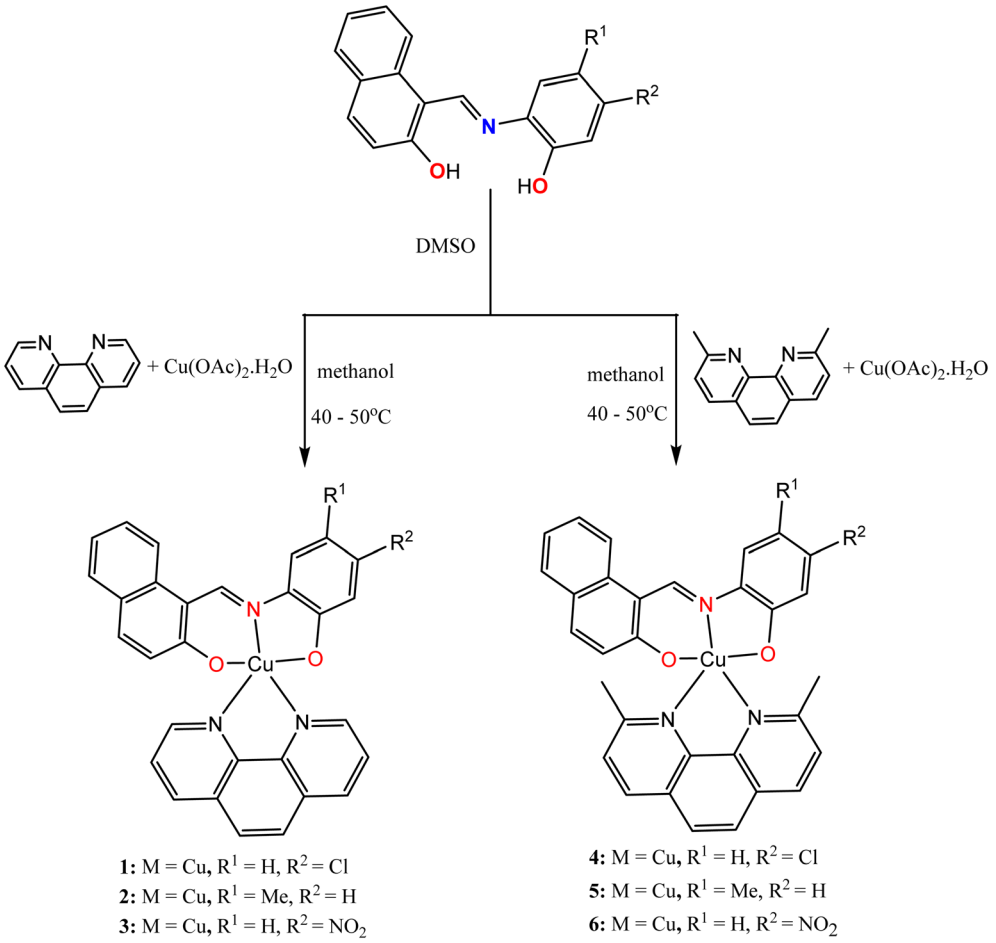

Scheme 1 Synthetic route for the preparation of complexes **1–6**.

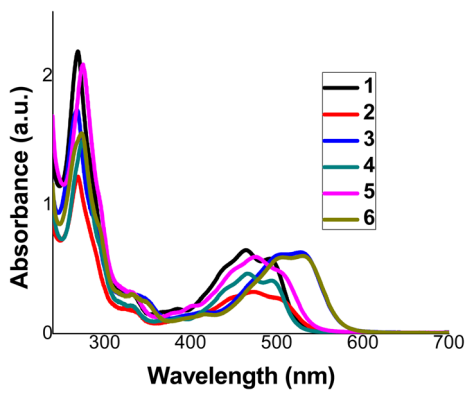

Fig. 1 Electronic absorption spectra of complexes **1–6**.

3.3 Single crystal X-ray structures

We used the single crystal X-ray crystallography technique to determine the structures of complexes **2**, **4**, **5** and **6**. Single crystals suitable for this experiment were obtained by the slow evaporation of 4 : 1 dichloromethane: methanol or chloromethane: methanol solution. Fig. 3 shows the crystal structures of the complexes using an ORTEP diagram with 50% probability thermal ellipsoids, while Table 2 details selected bond angles as well as bond lengths. Complexes **2**, **4** and **5** crystallize as monoclinic with a space group of $P2_1/c$ for complexes **2** and **4** and $P2_1/n$ for **5** while complex **6** crystallizes as triclinic with a space group of $P\bar{1}$. Generally, the asymmetric unit of the complexes contain a whole molecule with one molecule of solvent *i.e.* one molecule of dichloromethane for **2** and **6**, one molecule of chloromethane for **4**, and one molecule of methanol for **6**. All the crystal structures are mononuclear species in which the copper(II) ion is five-coordinated to a pair of oxygen atoms as well as one nitrogen atom from the Schiff base ligand (**L1–L3**) and to a pair of nitrogen atoms from the auxiliary ligand (1,10-phenanthroline or 2,9-dimethyl-1,10-phenanthroline) conforming to a distorted square pyramid with O1N7O2N1 atoms forming the basal plane for Cu1. The apical Cu1–N2 bond length for **2**, **5** and **6** and Cu1–N1 for **3** are longer than other two Cu–N bond lengths. For example, the Cu1–N2 bond length is 2.272(2)° in complex **2**, while the ones for Cu1–N1 as well as Cu1–N7 are 2.049(2)° and 1.944(2)° respectively. We used the structural parameter index (eqn (3)) for five coordinated complexes[51] to affirm the geometry of **2**, **4**, **5** and **6**.

$$\tau_5 = \frac{(\beta - \alpha)}{60} \quad (3)$$

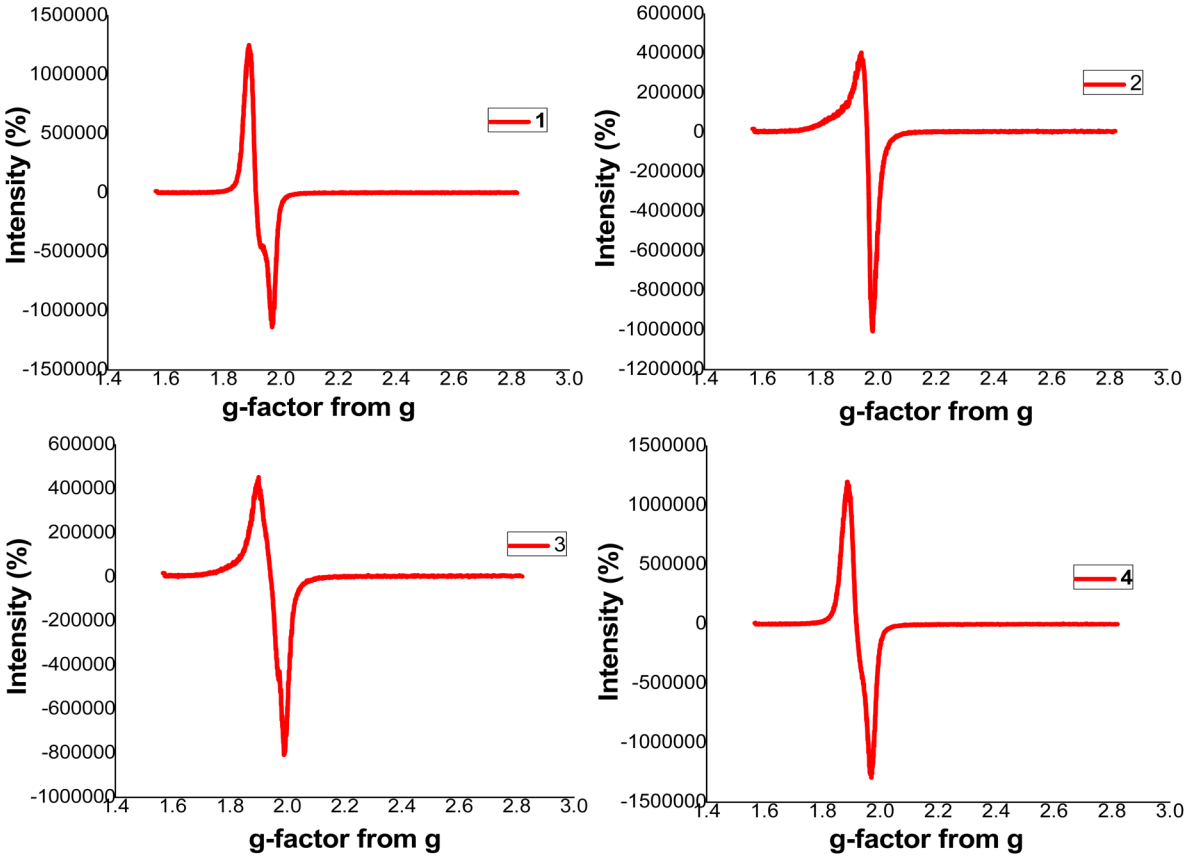

Fig. 2 ESR spectra of complexes **1–4**.

β and α are the largest coordination angles at the metal center. For $\tau_5 = 1$ and $\tau_5 = 0$, the geometries of the complex are trigonal bipyramidal and perfect square pyramidal, respectively. The calculated τ_5 values for complexes **2**, **4**, **5** and **6** are 0.01, 0.05, 0.04, and 0.05, respectively, and these fit into distorted square pyramidal attributed to the geometry of the complexes. The observed bond lengths and bond angles for the complexes are comparable to the ones of related copper(II) complexes with the same geometry.[52]

3.4 DNA binding study of ligands L1–L3 and complexes 1–6

The UV-visible absorption spectroscopy technique is commonly employed to study the noncovalent DNA binding modes for potential metallodrugs, particularly those targeting DNA replication in anticancer therapies. In this study, we evaluate the binding affinities of ligands **L1–L3** and complexes **1–6** to calf thymus DNA (ctDNA) by monitoring their spectral changes upon incremental ctDNA addition. All the compounds displayed absorption bands between 447 and 508 nm, showing hypochromism of 9.44–40.69% and bathochromic shifts of 2–9 nm with increasing ctDNA concentration (Fig. 4 and S15–S22). These observations suggest a potential intercalative binding, wherein the aromatic π-systems of the ligands stack with DNA base pairs, reducing transition probabilities. The pronounced hypochromism and red shifts signify strong π–π interactions, common in phenanthroline-containing copper complexes. Using the Wolfe–Shimmer equation (eqn (1)), the intrinsic binding constant (K_b) was calculated to quantify the binding interactions of the compounds.

The intrinsic binding constants (K_b) of **L1–L3** and complexes **1–6** (Table 3) revealed moderate to strong DNA affinities. The K_b values for **L1**, **L2** and **L3** were 1.49×10^4 M^{-1}, 2.46×10^4 M^{-1}, and 1.56×10^4 M^{-1}, respectively (**L2** > **L3** > **L1**; Table 3), reflecting the ligands' moderate DNA affinities.

Ligand **L2**, bearing a methyl substituent, exhibited the highest affinity due to enhanced π-electron density and hydrophobic interactions with DNA base pairs. In contrast, **L1** (chloro-substituted) and **L3** (nitro-substituted) showed lower affinities, likely due to the electron-withdrawing groups reducing π-stacking efficiency. Complexes **1–6** showed enhanced binding affinity, with K_b values ranging between 4.73×10^4 and 2.74×10^5 M^{-1} in the order **5** > **6** > **4** > **3** > **2** > **1**. Complex **5** exhibited the highest affinity (Fig. 4), attributable to the synergistic effect of the methyl group on its Schiff base ligand and the 2,9-dimethyl-1,10-phenanthroline coligand, which enhances hydrophobicity and π-stacking relative to unsubstituted phenanthroline.

The obtained K_b values of **1–6** show that the coordination of **L1–L3** to the copper(II) centre increased their binding affinities by 3 to 18-fold compared to the free ligands, suggesting metal-assisted stabilization of the potential intercalative mode. Notably, complexes **4–6** (with 2,9-dimethyl-1,10-phenanthroline

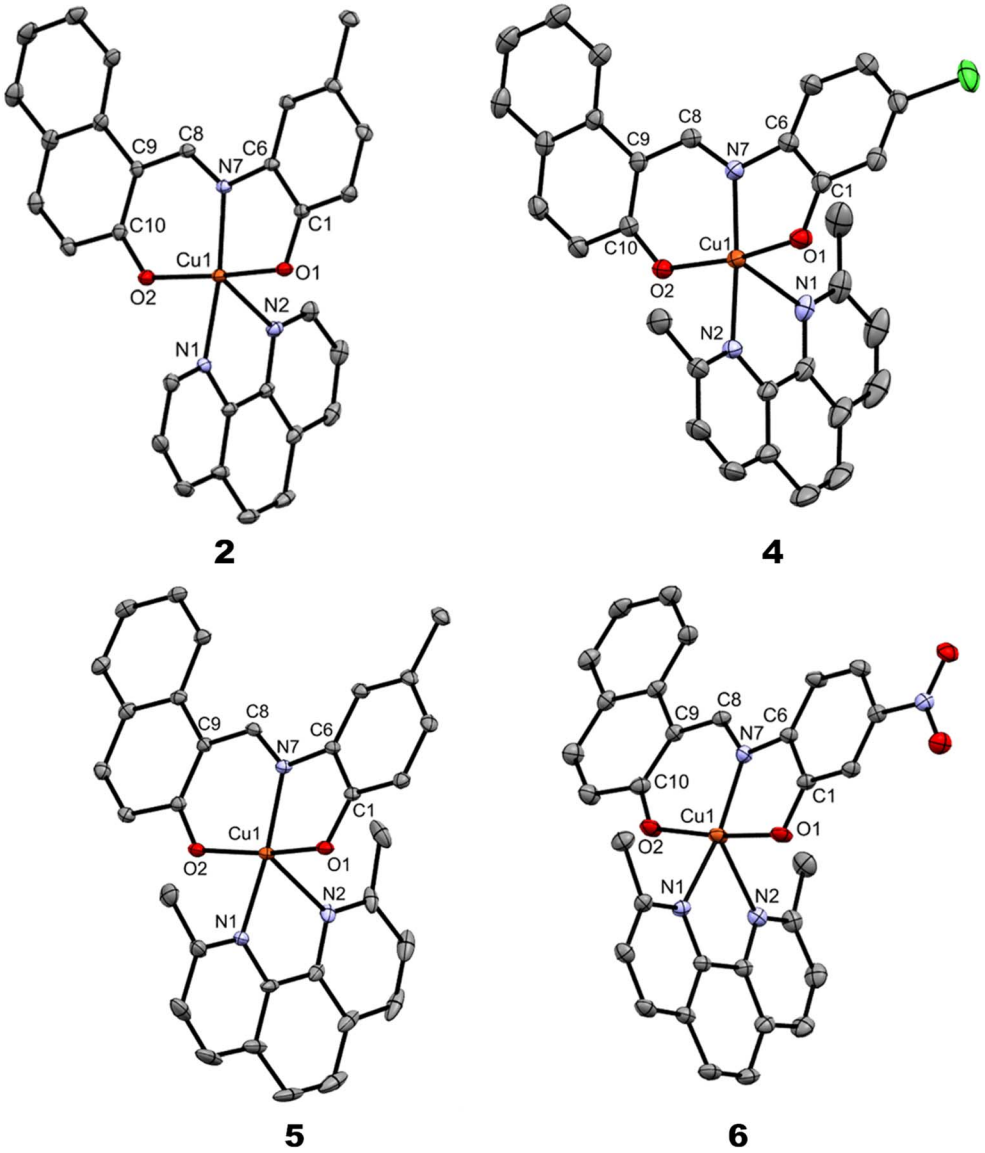

Fig. 3 Crystal structure of copper(II) complexes **2**, **4**, **5**, and **6** with thermal ellipsoids drawn at 50% probability. Hydrogen atoms were removed for clarity.

as co-ligand) show 2–3 times higher K_b values than **1–3**, due to methyl-induced hydrophobicity, as such encouraging π-stacking with DNA bases. Overall, the K_b values within 10^4–10^5 M^{-1} recorded for the compounds suggest their non-covalent intercalative binding modes, aligning with literature reports for mixed-ligand copper-phen Schiff base complexes (K_b = ~10^4–10^6 M^{-1}),[53,54] positioning these compounds as classical intercalators suitable for biomedical applications.

3.5 Bovine serum albumin interaction study

Drug molecule binding to plasma proteins offers useful information about drug distribution, transportation, and excretion, which is crucial in drug discovery and design. Bovine serum albumin (BSA), the most abundant plasma protein, serves as a cost-effective and structurally similar model to human serum albumin for drug–protein interaction studies. In this study, UV-visible absorption spectroscopy was employed to evaluate the binding affinity of copper(II) complexes **1–6** to BSA. The binding study was monitored by the conformational changes in BSA characterized by its intense absorbance at 280 nm, attributed to the polarity of tyrosine and tryptophan residues. Ligands **L1–L3** were excluded, as their ctDNA binding affinities were lower than those of the complexes.

Upon titration of increasing complexes **1–6** concentrations into fixed BSA solutions, continuous hyperchromic shifts were observed between 260 and 300 nm, with hyperchromism of 51.52–64.42% and hypsochromic shifts of 3–8 nm, indicating alterations in the protein microenvironment (Fig. 5 and S23–S27).

Binding constants (K_b) were calculated from the intercept-to-slope ratio of linear plots of $1/(A - A_0)$ *vs.* 1/[complex], where A

Table 2 Selected bond lengths (Å) and bond angles (°) for complexes **2**, **4**, **5** and **6**

Parameters	2	4	5	6
C8–N7	1.296(4)	1.294(4)	1.301(4)	1.311(4)
C10–O2	1.295(4)	1.302(4)	1.302(3)	1.298(5)
C1–O1	1.328(3)	1.321(4)	1.330(3)	1.316(4)
Cu1–O1	1.933(2)	1.977(2)	1.954(2)	1.942(3)
Cu1–O2	1.918(2)	1.930(2)	1.918(2)	1.911(3)
Cu1–N7	1.944(2)	1.945(3)	1.955(2)	1.955(3)
Cu1–N1	2.049(2)	2.303(2)	2.026(2)	2.052(3)
Cu1–N2	2.272(2)	2.045(3)	2.288(3)	2.323(4)
Bond angles				
O2–Cu1–O1	171.20(8)	168.09(9)	166.63(9)	171.4(1)
N2–Cu1–N1	77.75(8)	76.9(1)	78.0(1)	76.4(1)
N7–Cu1–O1	85.32(8)	83.68(9)	84.4(1)	84.6(1)
N7–Cu1–O2	92.23(8)	90.92(9)	92.4(1)	91.8(1)
O2–Cu1–N2	91.64(8)	91.2(1)	98.18(9)	92.0(1)
O1–Cu1–N1	90.18(8)	94.24(9)	91.6(1)	89.0(1)

and A_0 are the absorbances with and without complex, respectively. The K_b values for complexes **1–6** ranged from 9.59×10^4 M^{-1} to 2.41×10^5 M^{-1} (Table 3), falling within the typical 10^4 to 10^6 M^{-1} range for drug–protein interactions. This suggests their moderate to strong binding to protein, as such, suitable for pharmacological applications.

Complex **2** exhibited the highest binding affinity ($K_b = 2.41 \times 10^5$ M^{-1}, Fig. 5), followed by complex **1** (1.81×10^5 M^{-1}, Fig. S23) and complex **4** (1.57×10^5 M^{-1}, Fig. S24), highlighting the influence of ligand substituents and co-ligands. In complex **2** (bearing **L2** with an electron-donating methyl group on the aniline), the methyl group enhances lipophilicity, thus promoting stronger hydrophobic interactions and π–π stacking with BSA's aromatic residues in hydrophobic pockets like subdomain IIA. For complex **1**, the planarity of the unsubstituted 1,10-phenanthroline co-ligand could have influenced the insertion into the binding pocket. Similarly, complex **4**'s affinity can be related to the steric bulk and hydrophobic effects of the 2,9-dimethyl substituents on 1,10-phenanthroline, which promote stable interactions within the BSA subdomain. These trends correspond with literature reports on copper(II) Schiff base complexes, where substituents modulate binding through steric and electronic effects.[55,56] Overall, the K_b values position complexes **1–6**, especially **1**, **2**, and **4**, as viable drug carriers with protein, strong enough for transport and allowing free complex release for bioactivity.

3.6 *In vitro* antidiabetes activity

3.6.1 α-Amylase inhibition activity. In diabetes patients, α-amylase inhibitors are used to retard, or slow down dietary starch digestion, and this technique has been primarily used to manage type 2 diabetes by reducing post-meal blood sugar spikes.[57] Both the ligands (**L1–L3**) and the copper(II) complexes (**1–6**) displayed α-amylase inhibitory potential, and the results are quantified using IC_{50} values as shown in Table 4. The IC_{50} is the concentration of drug required for 50% inhibition. The lower the IC_{50} value, the better the α-amylase inhibitory efficiency. We observed that all the compounds displayed better α-amylase inhibition activity than the standard drug, acarbose, and the activity of the free ligands were greatly improved upon coordination with the copper(II) ion. For example, the IC_{50} for ligand **L1** is 0.78 mM while the one for complex **1** is 0.33 mM. It was suggested that this might be due to an increase in lipophilicity in **1–6** resulting from the complexation of the ligands with Cu^{2+}, which allowed them to penetrate through cell

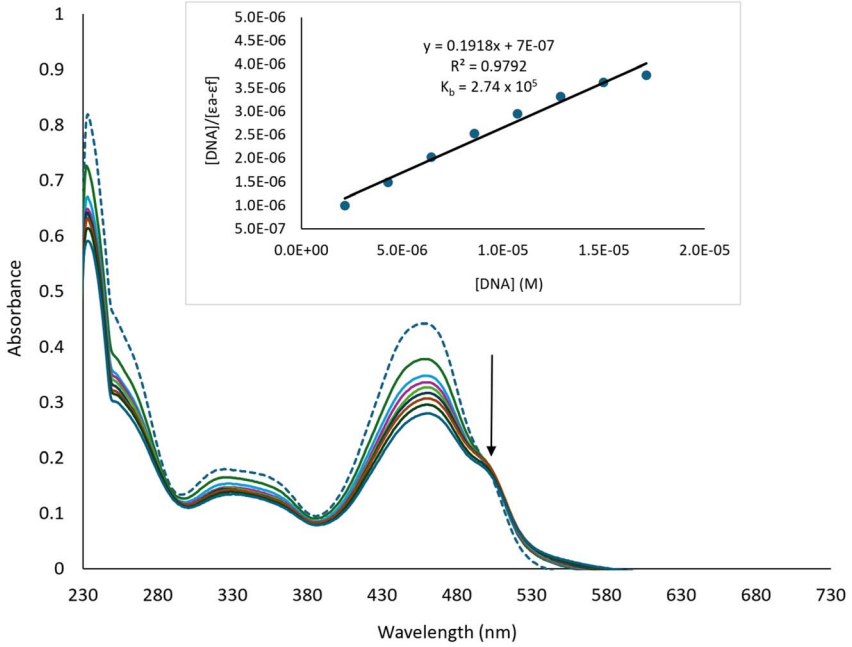

Fig. 4 Electronic absorption spectrum of complex **5** in the absence (dashed line) and the presence of different concentrations of ctDNA.

Table 3 The binding parameters of L1–L3 and complexes 1–6 interactions with CT-DNA and bovine serum albumin[a]

	DNA				BSA			
Cpd.	K_b ($\times 10^4$ M^{-1})	λ_{max} (nm)	Spec. Shift (nm)	%Hypo	K_b ($\times 10^5$ M^{-1})	λ_{max} (nm)	Spec. Shift (nm)	%Hyper
L1	1.49 ± 0.01	471	3(red)	40.69	—	—	—	—
L2	2.46 ± 0.06	446	3(red)	36.96	—	—	—	—
L3	1.56 ± 0.01	508	9(red)	9.44	—	—	—	—
1	4.73 ± 0.08	504	3(red)	30.63	1.81 ± 0.03	280	7(blue)	64.42
2	7.15 ± 0.01	483	2(red)	32.14	2.41 ± 0.06	280	4(blue)	51.52
3	9.31 ± 0.11	507	3(red)	22.83	1.53 ± 0.01	280	8(blue)	56.01
4	17.5 ± 0.20	462	2(red)	29.73	1.57 ± 0.07	280	3(blue)	61.55
5	27.4 ± 0.20	459	5(red)	36.65	1.46 ± 0.02	280	8(blue)	60.53
6	24.8 ± 0.05	490	3(red)	26.03	0.96 ± 0.03	280	4(blue)	54.28

[a] K_b = intrinsic binding constant; the K_b values shown are mean ± standard deviation.

membranes and reach targets (α-amylase) more easily compared to the unbound ligands.[58] However, further direct experimental evidence such as cellular uptake/penetration measurements must be carried out to ascertain this inference. It could also be observed that complexes with 2,9-dimethyl-1,10-phenanthroline showed good α-amylase inhibition activity than the ones having 1,10-phenanthroline in their structural backbone. This indicates that the electronic properties of the complexes play an important role in the inhibition of α-amylase. It was suggested that the presence of extra methyl moieties at position 2 and 9 of the 1,10-phenanthroline in complexes **4–6** might contribute to increased lipophilicity, which could, in turn, enhance their penetration and interaction with α-amylase enzymes compared to complexes **1–3** containing unsubstituted 1,10-phenanthroline. Statistically, the inhibitory activity of all

Table 4 Antidiabetic potential of free ligands L1–L3 and copper(II) complexes 1–6

	IC_{50} (mM)	
Compounds	α-Amylase	α-Glucosidase
L1	0.780	0.062
L2	0.415	0.071
L3	0.604	0.081
1	0.329	0.093
2	0.361	0.055
3	0.335	0.121
4	0.290	0.054
5	0.274	0.076
6	0.275	0.065
Acarbose	0.912	0.059

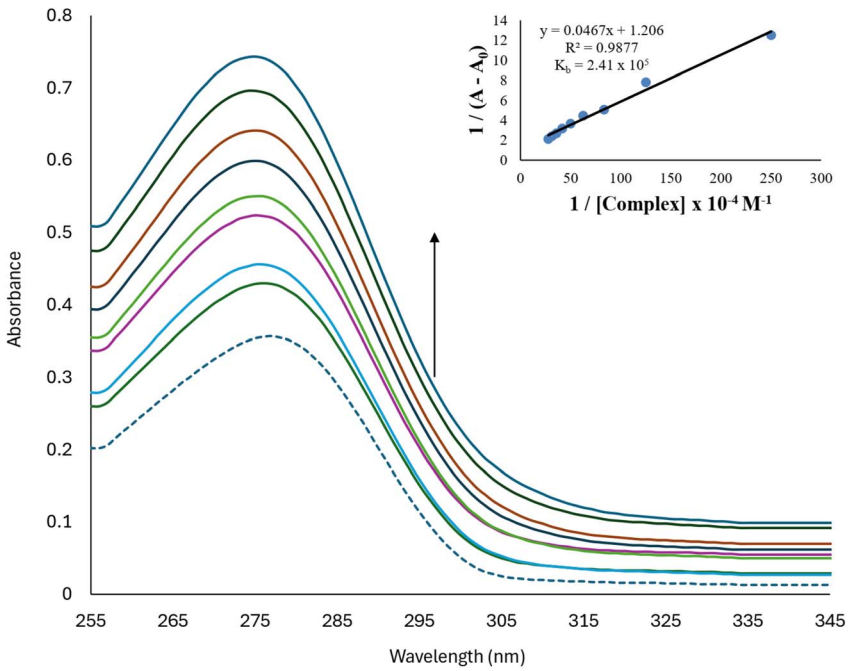

Fig. 5 Electronic absorption spectra of BSA in the absence (dashed line) and the presence of different concentrations of complex 2.

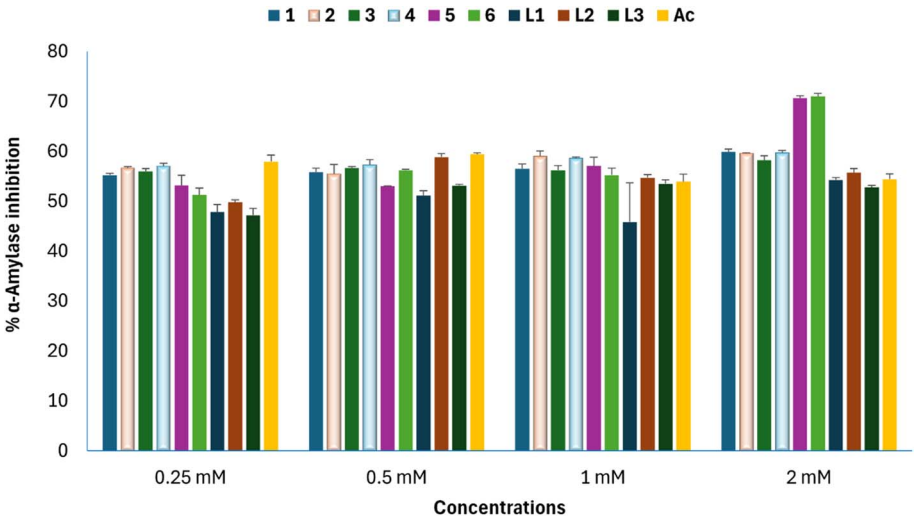

Fig. 6 Comparative α-amylase enzyme inhibitory effect of acarbose in comparison with the synthesised compounds at 0.25–2 mM test concentrations.

the compounds at a 0.5 mM test concentration ranges from 51% to 58%; however, at a 2 mM concentration, complexes **5** and **6** exhibited inhibitory activities of 70% and 71%, respectively (Fig. 6). This trend also reflected in their IC_{50} values. It could be generalized that, complexes **5** and **6** with IC_{50} values of 0.27 mM and 0.28 mM respectively, exhibited the best α-amylase enzyme inhibitory activities among the test samples.

3.6.2 α-Glucosidase inhibition activity. Another major strategy used in managing diabetes mellitus is to inhibit α-glucosidase, an enzyme also known as maltase.[59] α-Glucosidase catalyzes the breaking down of α(1 → 4) glycosidic bonds in starch, resulting in absorbable glucose in the body. Inhibiting the activities of α-glucosidase can directly reduce postprandial blood sugar in the body.[57] Herein, we studied the α-glucosidase inhibition capability of ligands **L1–L3** and complexes **1–6** and the results are given in Table 4. All the compounds displayed very good α-glucosidase inhibition potential. However, only complexes **2** and **4** with IC_{50} values of 0.055 mM and 0.054 mM outshined acarbose with IC_{50} value of 0.058 mM and this suggests that complexes **2** and **4** may have potential as antidiabetic therapeutics. Generally, as the concentration of the compounds increases, the % α-glucosidase inhibition increases, indicating that they are dose-dependent (Fig. 7). Contrary to what was observed for α-amylase inhibition assay, it cannot be outrightly stated that the complexes inhibited α-glucosidase better than the ligands, as there are few cases where the ligands performed better than the metal complexes. This might probably be due to ligands having superior access and binding affinities (*via* hydrogen bonding) to the enzyme active site when compared to ones of the respective copper(II) complex.

3.7 *In vitro* antioxidant activity

3.7.1 Nitric oxide inhibitory activity. The NO˙ assay is one of the important techniques used for evaluating antioxidant

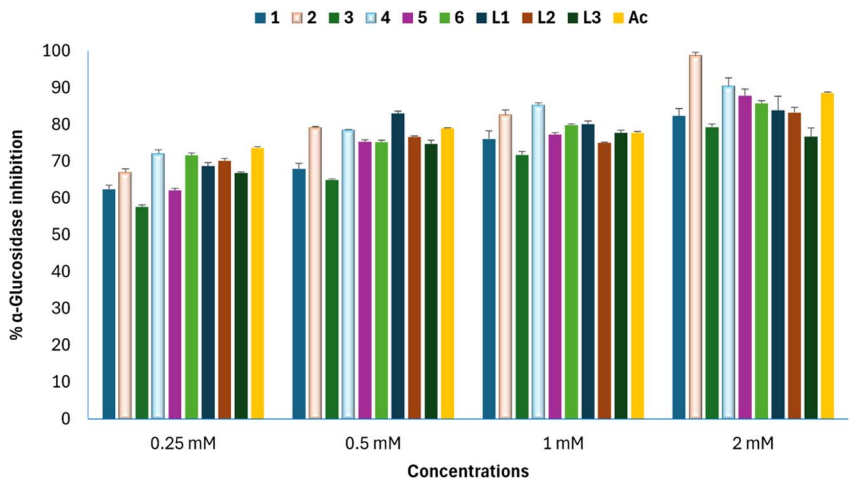

Fig. 7 Comparative α-glucosidase enzyme inhibitory effect of acarbose in comparison with the synthesized compounds at 0.25–2 mM test concentrations.

Table 5 Antioxidant potential of free ligands **L1–L3** and copper(II) complexes **1–6**

	IC_{50} (mM)		
Compounds	NO˙	DPPH	FRAP
L1	0.050	0.087	>5.00
L2	0.053	0.261	4.375
L3	0.050	0.531	3.414
1	0.066	0.627	>5.00
2	0.049	1.222	>5.00
3	0.079	1.323	>5.00
4	0.074	2.788	>5.00
5	0.065	1.001	>5.00
6	0.064	3.951	>5.00
Quercetin	0.060	0.126	0.034

activity of drug molecules due to the fact that it specifically assesses a compound's ability to scavenge reactive nitrogen species (RNS) and modulate inflammation, which are different from reactive oxygen species (ROS) handled by other assays.[60] Compounds capable of neutralizing nitric oxide radicals might be considered potential candidates for further investigation as anti-inflammatory agents. This is because chronic inflammatory conditions like arthritis are closely related to excessive nitric oxide radical. In this study, we evaluate the potential of free ligands **L1–L3** and copper(II) complexes **1–6** to scavenge NO˙ and the results are given in Table 5 and Fig. 8. All the compounds showed good NO˙ scavenging potential, and it was observed that all the ligands (**L1–L3**) as well as complex **2** outshined quercetin (the standard). While quercetin has an IC_{50} value of 0.060 mM, compounds **L1**, **L2**, **L3** and **2** have IC_{50} values of 0.050 mM, 0.053 mM, 0.050 mM and 0.049 mM respectively. Generally, the ligands scavenge NO˙ better than the complexes. This might be due to the masking of the hydroxyl group (electron-donating group) in the complexes, which ought to have facilitated electron transfer and in turn stabilizes NO˙.

3.7.2 DPPH free radical neutralising ability. The antioxidant potential of the ligands (**L1–L3**) as well as their corresponding copper(II) complexes (**1–6**) were also evaluated using the DPPH free radical scavenging assay, and the results were expressed as IC_{50} values as given in Table 5. The antioxidant activities of the compounds were compared to quercetin. All the ligands showed good results. Among all the compounds, **L1** exhibited the strongest activity, with an IC_{50} value of 0.087 mM, which is lower than that of other compounds and quercetin (0.126 mM) inclusive. Similarly to what was observed in the nitric oxide assay, the ligands scavenge the free radical of DPPH better than that of the copper(II) complexes. The reduced antioxidant potential observed for the complexes **1–6** might be attributed to the coordination of the ligand donor atoms to the metal center, which can limit the availability of the hydroxyl group or heteroatom sites responsible for effective hydrogen atom or electron transfer to the DPPH free radicals.[61] More so, steric hindrance and changes in electronic distribution following the coordination of copper(II) with the ligands may further impede interaction with the free radical species. Generally, the % free radical scavenging of the compounds increases as the concentration increases from 0.25 mM to 2.00 mM (Fig. 9).

3.7.3 Ferric ion reducing capacity assay. We used the ferric ion reductive capacity assay to further investigate the compounds' potential as antioxidants. Antioxidants can generally convert ferric ions (Fe^{3+}) to ferrous ions (Fe^{2+}), and the reduction transformation level can be used to assess the antioxidant capability.[62] The data in Fig. 10 revealed that at test concentrations ranging from 0.25 to 2 mM, complexes **1–6** exhibited lower Fe^{3+} reducing properties than compounds **L1–L3**. While compounds **L1**, **L2**, and **L3** at 1 mM had estimated activities of approximately 28%, 37%, and 40%, respectively, these properties increased by 52%, 36%, and 37% at the highest test concentration. Despite the antioxidant potency of these synthesized compounds, they could not outperform quercetin, which had higher activities at 2 mM. Nonetheless, the results in Table 5 showed that compounds **L2**, **L3** and quercetin had IC_{50} values of 4.375 mM, 3.414 mM, and 0.034 mM, respectively,

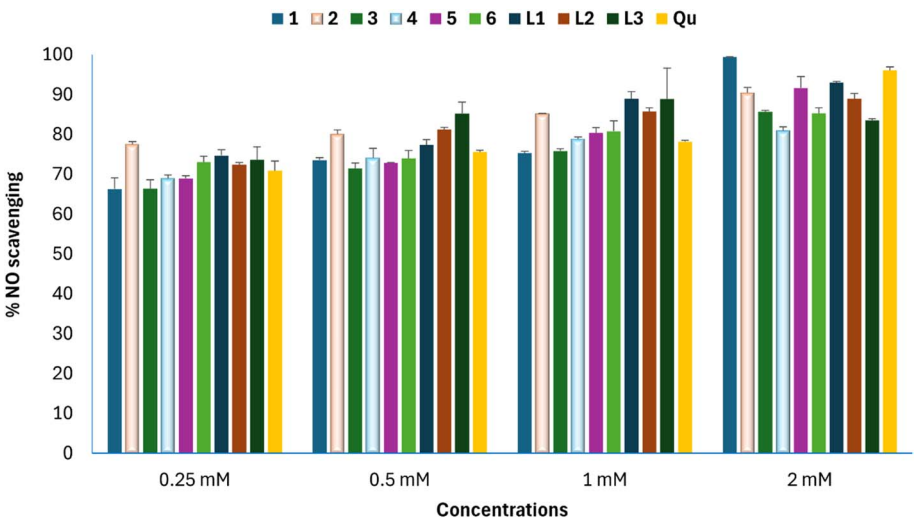

Fig. 8 Effect of the compounds in comparison with quercetin to inhibit nitric oxide formation at 0.25–2 mM test concentrations.

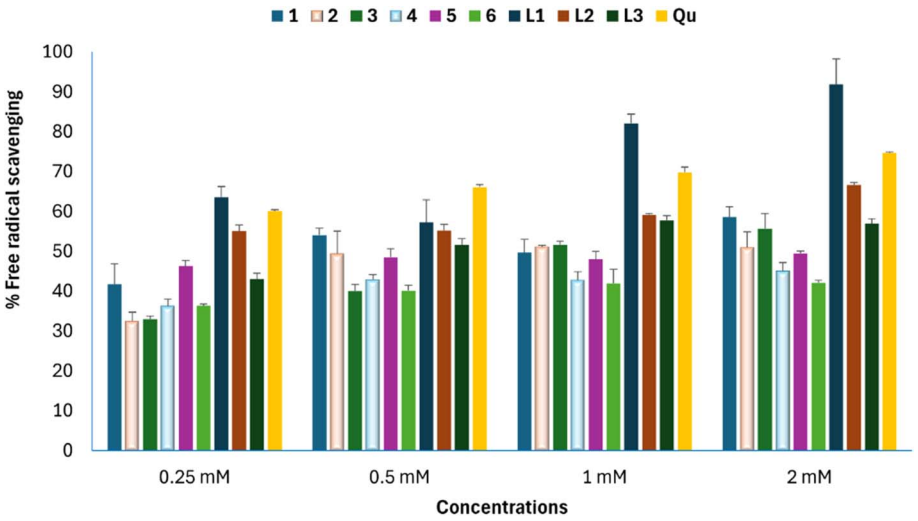

Fig. 9 Free radical scavenging effect of quercetin in comparison with the compounds at 0.25–2 mM test concentrations.

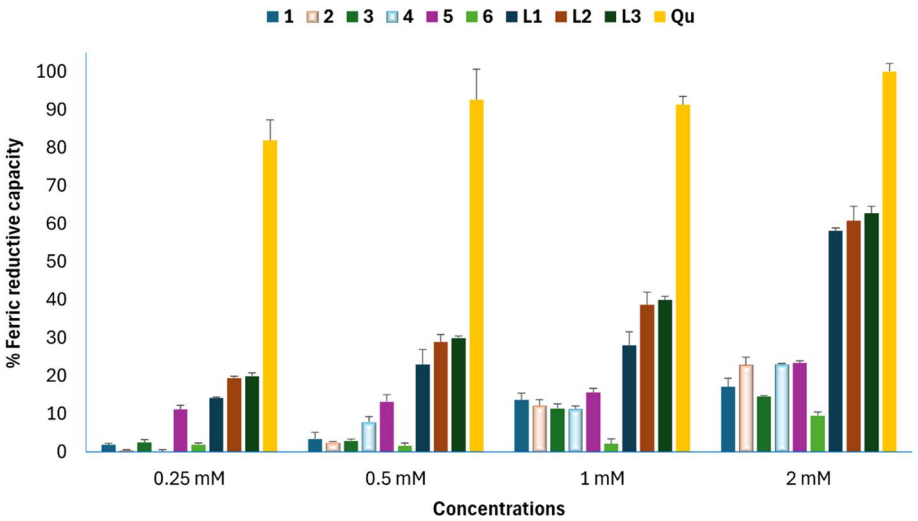

Fig. 10 Fe^{3+} reducing effect of quercetin in comparison with the compounds at 0.25–2 mM test concentrations.

while others have IC_{50} values greater than 5.00 mM. The IC_{50} values obtained for complexes **1–6** indicate that, they exhibited very weak or negligible ferric reducing ability under the experimental conditions used for this study.

4 Conclusion

In conclusion, six new copper(II) complexes derived from mixed ligands (Schiff bases and diimines) with general molecular formula [Cu**L1**(Phen/DM-Phen)] have been synthesized and characterized by core spectroscopic techniques. The crystallography analysis of complexes **2**, **4**, **5** and **6** unraveled the geometry around the CuO_2N_3 of the complexes to be distorted square pyramidal. UV-visible absorption spectroscopy revealed the interactions of ligands **L1–L3** and complexes **1–6** with ctDNA and BSA. Spectral analysis showed hypochromism with slight bathochromic shifts, suggesting an intercalation binding mode with ctDNA *via* classical non-covalent π-stacking. Complexes **1–6** displayed moderate-to-strong binding affinities to ctDNA (K_b = 4.73 × 10^4 to 2.74 × 10^5 M^{-1}), better than those of the free ligands **L1–L3** (K_b = 1.49 × 10^4 to 2.46 × 10^4 M^{-1}). This positions the complexes as promising DNA-targeting agents for anticancer applications. For BSA, complexes **1–6** exhibited strong binding (K_b = 9.59 × 10^4 to 2.41 × 10^5 M^{-1}), accompanied by hyperchromic shifts that signal microenvironment alterations and hydrophobic/π–π interactions, particularly driven by lipophilic methyl substituents (highest in complex **2**). These affinities lie within optimal pharmacological ranges, facilitating effective protein-potential drug transport and release for bioactivity, especially for complexes **1**, **2**, and **4**. All the complexes displayed good α-amylase and α-glucosidase inhibition potential with complexes **2** and **4** having lower IC_{50} values than the ones for acarbose in both assays, suggesting them to have potential as antidiabetic therapeutics.

Compounds with methyl group substituents displayed better DNA and BSA binding affinities when compared to those with chloro and nitro groups. They also inhibit α-amylase and α-glucosidase more than their counterparts. The ligands exhibited good antioxidant activities compared to copper(II) complexes and also scavenge nitric oxide and DPPH (only **L1**) radical better than quercetin, the standard used for this study.

Author contributions

Conceptualization, S. D. O. and R. C. L.; methodology; S. D. O., A. A. A., B. O. R. C. L. and K. A. O.; software, S. D. O., K. A. O., and A. A. A., validation, S. D. O., A. A. A., K. A. O., B. O., and R. C. L.; formal analysis; S. D. O., K. A. O., and A. A. A.; resources' R. C. L., B. O., data curation, S. D. O, A. A. A. and K. A. O.; writing original draft preparation; S. D. O., A. A. and K. A. O.; writing review and editing, S. D. O., A. A. A., K. A. O., B. O. and R. C. L., visualization, S. D. O., A. A. A., K. A. O., B. O., and R. C. L., supervision, R. C. L., project administration, R. C. L., funding acquisition, S. D. O and R. C. L.

Conflicts of interest

The authors declare no conflicts of interest.

Data availability

CCDC 2530540 (**2**), 2530541 (**4**), 2530542 (**5**) and 2530543 (**6**) contain the supplementary crystallographic data for this paper.[63a–d]

All data generated or analyzed during this study are included in this published article and its supplementary information (SI). Supplementary information (with charaterization data) is available. See DOI: https://doi.org/10.1039/d6ra01650b.

Acknowledgements

The authors acknowledge the funding from the National Research Foundation (grant number: CPRR23041794158), Stellenbosch University, Matieland, 7602, South Africa. The first author is a recipient of a postdoctoral fellowship award of the NRF at Stellenbosch University, Matieland, South Africa.

References

1 A. A. Ali, M. Shebl, O. M. Adly, M. S. Mahfouz and R. Fouad, *J. Mol. Struct.*, 1359, **206**, 145313.
2 S. D. Oladipo, B. Omondi and C. Mocktar, *Polyhedron*, 2019, **170**, 712–722.
3 L. Esmaeili, M. G. Perez, M. Jafari, J. Paquin, P. Ispas-Szabo, V. Pop, M. Andruh, J. Byers and M. A. Mateescu, *J. Inorg. Biochem.*, 2019, **192**, 87–97.
4 I. Bento, C. Peixoto, V. N. Zaitsev and P. F. Lindley, *Acta Crystallogr., Sect. D:Biol. Crystallogr.*, 2007, **63**, 240–248.
5 F. Tisato, C. Marzano, M. Porchia, M. Pellei and C. Santini, *Med. Res. Rev.*, 2010, **30**, 708–749.
6 X. Wu, Y. Zhou, Z. Lu, Y. Zhang, T. Zhang and Q. Jiang, *Anim. Biosci.*, 2024, **38**, 530.
7 M. Azeem, K. Li, Y. Qin, L. Dong and W. Li, *CrystEngComm*, 2021, **23**, 1815–1820.
8 I. Iakovidis, I. Delimaris and S. M. Piperakis, *Mol. Biol. Int.*, 2011, **2011**, 594529.
9 S. D. Oladipo, R. C. Luckay, K. A. Olofinsan, A. A. Badeji and S. Mokoena, *Inorg. Chim. Acta*, 2025, **575**, 122447.
10 T. L. Yusuf, I. Waziri, S. D. Oladipo, M. S. Abd El-Maksoud, A. J. Muller and B. Vatsha, *ACS Omega*, 2025, **10**, 50795–50805.
11 S. D. Oladipo, R. C. Luckay and K. A. Olofinsan, *Results Chem.*, 2025, **16**, 102471.
12 S. Thakur, A. Jaryal and A. Bhalla, *Results Chem.*, 2024, **7**, 101350.
13 M. E. Moreno-Narváez, L. González-Sebastián, R. Colorado-Peralta, V. Reyes-Márquez, L. O. Franco-Sandoval, A. Romo-Pérez, J. A. Cruz-Navarro, I. V. Mañozca-Dosman, A. Aragón-Muriel and D. Morales-Morales, *Inorganics*, 2025, **13**, 38.
14 R. D. Mohan, S. Sarukrishna, A. S. Babu, D. Santhosh, S. A. Fathima and B. Parvathy, *Inorg. Chim. Acta*, 2026, **550**, 122980.
15 A. Gil, M. Melle-Franco, V. Branchadell and M. J. Calhorda, *J. Chem. Theor. Comput.*, 2015, **11**, 2714–2728.
16 M. A. Alossaimi, T. Aldakhil, H. Elmansi, F. Belal and G. Magdy, *RSC Adv.*, 2026, **16**, 5437–5454.
17 X.-B. Fu, D.-D. Liu, Y. Lin, W. Hu, Z.-W. Mao and X.-Y. Le, *Dalton Trans.*, 2014, **43**, 8721–8737.
18 J. C. García-Ramos, R. Galindo-Murillo, F. Cortés-Guzmán and L. Ruiz-Azuara, *J. Mex. Chem. Soc.*, 2013, **57**, 245–259.
19 D. Ray, A. Manna, M. F. Ansari, F. Arjmand, Z. Jaglicic and R. Herchel, *Dalton Trans.*, 2026, **55**, 3750.
20 R. Ghanta, S. Jhulki, T. Chowdhury, P. Giri, R. Mondal, S. Kundu, S. Dasgupta, U. K. Das, M. Jana and A. Pal, *Appl. Organomet. Chem.*, 2026, **40**, e70511.
21 S. V. Saravanaselvam, X. Arulanantham, M. Tamilelakkiya, R. Sakthivadivel, S. Ponnusamy, P. Pandi, P. Velusamy, S. E. Muthu and K. A. Kumar, *J. Mol. Struct.*, 2025, **1325**, 141000.
22 M. Lištiak, J. Valentová, E. Zahradníková, R. Varga, E. Samoľová, M. Litecká, K. Lušpai, M. Puchoňová, M. Malček Šimunková and J. Moncoľ, *Eur. J. Inorg. Chem.*, 2025, **28**, e202500143.
23 V. Vinayagam, D. Chandren, P. Arthur, S. Theerthagiri and W. Yong, *Inorg. Chem. Commun.*, 2024, **161**, 112116.
24 M. Maity, U. Pramanik, V. R. Hathwar, P. Brandao, S. Mukherjee, S. Maity, R. Maity, T. Maity and B. C. Samanta, *Heliyon*, 2022, **8**, e11345.
25 N. Yasumatsu, Y. Yoshikawa, Y. Adachi and H. Sakurai, *Bioorg. Med. Chem.*, 2007, **15**, 4917–4922.
26 S. D. Oladipo and R. C. Luckay, *New J. Chem.*, 2024, **48**, 13276–13288.
27 S. S. Lakshmi, K. Geetha, M. Gayathri and G. Shanmugam, *J. Chem. Sci.*, 2016, **128**, 1095–1102.
28 T. S. Chaithanya and V. Sabareesh, *Pept. Sci.*, 2026, **118**, e70017.

29 A. Reuser and H. Wisselaar, *Eur. J. Clin. Invest.*, 1994, **24**, 19–24.
30 S. R. Pathak, K. R. Senwar and K. N. Sharma, in *Diabetes Mellitus*, Elsevier, 2025, pp. 63–78.
31 M. Sabu and R. Kuttan, *J. Ethnopharmacol.*, 2002, **81**, 155–160.
32 P. Thakur, A. Kumar and A. Kumar, *J. Drug Targeting*, 2018, **26**, 766–776.
33 A. Ceriello, *Diabetes Care*, 2003, **26**, 1589–1596.
34 M. Valko, C. Rhodes, J. Moncol, M. Izakovic and M. Mazur, *Chem.-Biol. Interact.*, 2006, **160**, 1–40.
35 T. Dhanya, M. P. Kurup, K. Rajimon, G. A. Krishna, J. K. Varughese, K. Raghu, S. Philip, K. Divya, M. Augustine and P. Mohanan, *Dalton Trans.*, 2025, **54**, 3216–3234.
36 S. D. Oladipo, R. C. Luckay, A. A. Badeji, V. A. Obakachi, K. K. Govender and A. D. Osinubi, *Chem. Biodiversity*, 2026, **23**, e02739.
37 T. Kiran, V. G. Prasanth, M. Balamurali, C. Vasavi, P. Munusami, K. I. Sathiyanarayanan and M. Pathak, *Inorg. Chim. Acta*, 2015, **433**, 26–34.
38 *APEX4, SAINT, and SADABS*, Bruker AXS Inc., Madison, WI, 2022.
39 G. M. Sheldrick, *Acta Crystallogr., Sect. A: Found. Adv.*, 2015, **71**, 3–8.
40 L. J. Barbour, *J. Appl. Crystallogr.*, 2020, **53**, 1141–1146.
41 C. F. Macrae, I. Sovago, S. J. Cottrell, P. T. Galek, P. McCabe, E. Pidcock, M. Platings, G. P. Shields, J. S. Stevens and M. Towler, *J. Appl. Crystallogr.*, 2020, **53**, 226–235.
42 A. A. Adeleke, Md. S. Islam, K. Olofinsan, V. F. Salau, C. Mocktar and B. Omondi, *New J. Chem.*, 2021, **45**, 17827–17846.
43 T. L. Yusuf, D. C. Akintayo, S. D. Oladipo, A. A. Adeleke, K. Olofinsan, B. Vatsha and N. Mabuba, *New J. Chem.*, 2022, **46**, 12968–12980.
44 S. J. Zamisa, A. A. Adeleke, N. Devnarain, M. A. Rhman, P. M. O. Owira and B. Omondi, *RSC Adv.*, 2023, **13**, 21820–21837.
45 O. Ibitoye, K. Olofinsan, K. Teralı, U. Ghali and T. Ajiboye, *J. Food Biochem.*, 2018, **42**, e12627.
46 K. A. Olofinsan, O. L. Erukainure, N. Z. Msomi and M. S. Islam, *Asian Pac. J. Trop. Biomed.*, 2022, **12**, 300–311.
47 B. K. Beseni, K. A. Olofinsan, V. F. Salau, O. L. Erukainure and M. S. Islam, *Asian Pac. J. Trop. Biomed.*, 2022, **12**, 453–465.
48 P. Changlian, C. Shaowei, L. Zhifang and L. Guizhu, *Europe PMC*, 2000, **27**, 658–661.
49 M. K. Koley, S. U. Parsekar, N. Duraipandy, M. S. Kiran, B. Varghese, P. T. Manoharan and A. P. Koley, *Inorg. Chim. Acta*, 2018, **478**, 211–221.
50 W. A. Munzeiwa, S. D. Oladipo, C. U. Ibeji, C. Mocktar and B. Omondi, *J. Inorg. Biochem.*, 2021, **225**, 111600.
51 A. W. Addison, T. N. Rao, J. Reedijk, J. van Rijn and G. C. Verschoor, *J. Chem. Soc., Dalton Trans.*, 1984, 1349–1356.
52 B. Mohan and M. Choudhary, *J. Mol. Struct.*, 2021, **1246**, 131246.
53 K. Paliwal, P. Haldar, P. K. S. Antharjanam and M. Kumar, *ACS Omega*, 2022, **7**, 21961–21977.
54 L. Li, Q. Guo, J. Dong, T. Xu and J. Li, *J. Photochem. Photobiol., B*, 2013, **125**, 56–62.
55 S. Mali, S. D. Vatagude, M. Horitani and P. M. Gurubasavaraj, *J. Mol. Struct.*, 2026, **1360**, 145599.
56 S. K. Tarai, S. Mandal, A. Tarai, I. Som, A. Pan, A. Bagchi, A. Biswas and S. C. Moi, *Appl. Organomet. Chem.*, 2023, **37**, e7164.
57 H. O. Omoregie, T. L. Yusuf, S. D. Oladipo, K. A. Olofinsan, M. B. Kassim and S. Yousuf, *Polyhedron*, 2022, **217**, 115738.
58 A. d. S. Portas, D. C. Miguel, J. K. Yokoyama-Yasunaka, S. R. B. Uliana and B. P. Espósito, *J. Biol. Inorg. Chem.*, 2012, **17**, 107–112.
59 S. D. Oladipo, R. C. Luckay, K. A. Olofinsan, V. A. Obakachi, S. J. Zamisa, A. A. Adeleke, A. A. Badeji, S. A. Ogundare and B. P. George, *Heliyon*, 2024, **10**, e23174.
60 U. Rao, B. A. Ahmad and K. S. Mohd, *Malays. J. Anal. Sci.*, 2016, **20**, 1191–1202.
61 E. Rodríguez-Arce and M. Saldías, *Biomed. Pharmacother.*, 2021, **143**, 112236.
62 İ. Gulcin and S. H. Alwasel, *Processes*, 2025, **13**, 1296.
63 (*a*) CCDC 2530540: Experimental Crystal Structure Determination, 2026, DOI: 10.5517/ccdc.csd.cc2qy7b8; (*b*) CCDC 2530541: Experimental Crystal Structure Determination, 2026, DOI: 10.5517/ccdc.csd.cc2qy7c9; (*c*) CCDC 2530542: Experimental Crystal Structure Determination, 2026, DOI: 10.5517/ccdc.csd.cc2qy7db; (*d*) CCDC 2530543: Experimental Crystal Structure Determination, 2026, DOI: 10.5517/ccdc.csd.cc2qy7fc.